

Article

Synthesis and Characterization of Ni–Co–O Nanosheets on Silicon Carbide Microspheres/Graphite Composite for Supercapacitor Applications

Han-Wei Chang^{1,2,*} , Zong-Ying Tsai³, Jia-Jun Ye¹, Kuo-Chuang Chiu⁴, Tzu-Yu Liu⁴ and Yu-Chen Tsai^{3,*}

¹ Department of Chemical Engineering, National United University, Miaoli 360302, Taiwan; u0914010@o365.nuu.edu.tw

² Pesticide Analysis Center, National United University, Miaoli 360302, Taiwan

³ Department of Chemical Engineering, National Chung Hsing University, Taichung 402202, Taiwan; g111065070@mail.nchu.edu.tw

⁴ Material and Chemical Research Laboratories, Industrial Technology Research Institute, Hsinchu 310401, Taiwan; ckc@itri.org.tw (K.-C.C.); jill.t.y.liu@itri.org.tw (T.-Y.L.)

* Correspondence: hwchang@nuu.edu.tw (H.-W.C.); yctsai@dragon.nchu.edu.tw (Y.-C.T.); Tel.: +886-37-382216 (H.-W.C.); +886-4-22857257 (Y.-C.T.)

Abstract: The well-interconnected ternary Ni–Co–O nanosheets were grown on silicon carbide microspheres/graphite composite (gra@SiC/Ni–Co–O) by optimizing the electrodeposition method. Silicon carbide microspheres/graphite composite (gra@SiC) serves as a conductive template for the growth of Ni–Co–O nanosheets to form a binder-free 3D well-designed hierarchical interconnected network between the Ni–Co–O nanosheets and SiC microspheres. The obtained gra@SiC/Ni–Co–O is proposed as a great capacitance performance for supercapacitors. Field emission scanning electron microscopy (FESEM), Raman spectroscopy, high-resolution transmission electron microscopy (HRTEM) with selected area electron diffraction (SAED) and energy dispersive X-ray spectroscopy (EDS), X-ray photoelectron spectroscopy, and electrochemical analysis were employed to investigate the morphology and structural and electrochemical characteristics. The synergistic effects of EDLC (SiC microspheres) and pseudo-capacitance (Ni–Co–O nanosheets) can effectively improve the supercapacitive performance. It is also worth mentioning that after electrochemical testing, the redox reaction of Ni–Co–O nanosheets greatly promoted the faradic pseudo-capacitance contribution, and silicon carbide microspheres/graphite composite contributed to the formation of a 3D interconnected network, improving the cycling stability during the charging/discharging processes.

Keywords: ternary Ni–Co–O nanosheets; silicon carbide microspheres/graphite composite; supercapacitor; EDLC and pseudo-capacitance



Citation: Chang, H.-W.; Tsai, Z.-Y.; Ye, J.-J.; Chiu, K.-C.; Liu, T.-Y.; Tsai, Y.-C. Synthesis and Characterization of Ni–Co–O Nanosheets on Silicon Carbide Microspheres/Graphite Composite for Supercapacitor Applications. *C* **2023**, *9*, 101. <https://doi.org/10.3390/c9040101>

Academic Editors: Gil Gonçalves and Olena Okhay

Received: 3 October 2023

Revised: 22 October 2023

Accepted: 27 October 2023

Published: 29 October 2023



Copyright: © 2023 by the authors. Licensee MDPI, Basel, Switzerland. This article is an open access article distributed under the terms and conditions of the Creative Commons Attribution (CC BY) license (<https://creativecommons.org/licenses/by/4.0/>).

1. Introduction

Resource depletion, extreme climate change, and environmental damage are the major driving forces for the development of renewable and sustainable energy technologies (e.g., supercapacitors, fuel cells, hydrogen generation, and rechargeable batteries) [1–3]. As promising energy storage devices, supercapacitors have attracted significant research interest among researchers owing to their high power density, fast charge/discharge rate, excellent reversibility, and high durability. Additionally, they can be integrated into hybrid energy storage systems to meet the demand for renewable energy sources that can address the aforementioned issues. The charge storage mechanisms of supercapacitors are mainly divided into electrochemical double-layer capacitance (EDLC) and pseudo-capacitance. The EDLC accumulates the charges at the interface between the electrode and electrolyte through non-Faradaic physical processes. Carbon, semiconductor, and cermet materials are widely used as electrode materials in EDLC supercapacitors [4–6]. The performance of pseudo-capacitance is derived from the pseudocapacitive materials through

Faradaic processes involving surface or near-surface redox reactions. Transition metal-based compounds are considered the most ideal electrode materials for pseudocapacitance. Generally, binary and ternary transition metal compounds as electrode materials have been widely investigated due to their rich redox chemistry and valence state transitions, promising pseudocapacitive characteristics [7–9].

Particularly, the unique tuneable bandgaps of silicon carbide (SiC) EDLC-type semiconductor electrode materials enable high electron mobility, good mechanical performance, and excellent temperature stability, indicating that it may be a good candidate for supercapacitor electrode materials. However, the relatively low energy density of SiC-based materials for EDLC limits their applicability in supercapacitors. Hybrid supercapacitors combine the intrinsic properties of both EDLC and pseudo-capacitance to solve the existing limitation of EDLC to significantly improve the supercapacitor performance. Significant efforts have been devoted to combining SiC-based EDLC and transition metal-based pseudo-capacitance-type materials as electrode materials for supercapacitors. A previous study reported that the combination of microspherical SiC as EDLC materials and birnessite-type MnO_2 as pseudo-capacitance materials provides an effective method to achieve high supercapacitor performance compared to the performance of microspherical SiC used in EDLC. Typically, SiC should possess a high surface area to enable its use as support structures for the growth of birnessite-type MnO_2 with intimate interfacial contact, significantly facilitating the electrons and ions transportation in the electrode, resulting in excellent capacitive performance [10]. Another study reported that the obtained ferroferric oxide (Fe_3O_4) grown on SiC flakes ($\text{Fe}_3\text{O}_4/\text{SiC}$) is a feasible configuration for supercapacitors, as the introduction of Fe_3O_4 into the composite significantly enhanced the capacitive performance of the SiC, which can be attributed to the additional pseudo-capacitance contributed by the Fe_3O_4 [11]. Further, another study synthesized $\text{MgCo}_2\text{O}_4/\text{SiC}$ composite as an electrode material for supercapacitors by growing ternary transition metal oxides (spinel cobaltites (MgCo_2O_4)) on SiC flakes. The synergistic effects of the EDLC behavior of SiC and the pseudo-capacitance behavior of MgCo_2O_4 enhanced the supercapacitive performance of the composite. In particular, they observed that SiC provided a more accessible surface area for charge storage through ion adsorption to further enhance the capacitance of the EDLC, and MgCo_2O_4 simultaneously exhibited pseudo-capacitive energy storage efficiency through the multiple oxidation states/structures of Mg and Co ions [12]. The findings of the aforementioned studies indicated that hybrid supercapacitors (EDLC and pseudo-capacitance) can be fabricated by incorporating SiC with transition metal-based compounds, thus presenting a feasible strategy to enhance the capacitance of supercapacitors.

In this work, well-interconnected ternary Ni–Co–O nanosheets were directly grown on silicon carbide microspheres (gra@SiC/Ni–Co–O) by optimizing the electrodeposition method. Silicon carbide (SiC) possesses excellent surface characteristics, electron mobility, mechanical performance, and temperature stability to exhibit better EDLC properties. A simple and low-cost electrodeposition method is suitable for the preparation of binder-free electrode materials without adding conductive agents and binders. Observations revealed that the Ni–Co–O nanosheets were uniformly grown on the surface of silicon carbide microspheres using a binder-free electrodeposition process, which enabled the maximal exposure of active sites, thus ensuring sufficient charge transport kinetics at the electrode/electrolyte interface. Simultaneously, the synergistic effect between the Ni–Co–O nanosheets and silicon carbide microspheres further endowed the EDLC of silicon carbide microspheres with the additional pseudocapacitance of Ni–Co–O nanosheets. This study demonstrated the promising potential of the designed gra@SiC/Ni–Co–O and provided guidelines for enhancing the capacitance of SiC-based supercapacitors.

2. Materials and Methods

2.1. Reagents

Nickel(II) chloride hexahydrate ($\text{NiCl}_2 \cdot 6\text{H}_2\text{O}$), nickel(II) nitrate hexahydrate ($\text{Ni}(\text{NO}_3)_2 \cdot 6\text{H}_2\text{O}$), cobalt(II) nitrate hexahydrate ($\text{Co}(\text{NO}_3)_2 \cdot 6\text{H}_2\text{O}$), and potassium hydroxide (KOH) were purchased from Sigma-Aldrich (St. Louis, MO, USA). Silicon carbide (SiC) was provided by the Industrial Technology Research Institute (ITRI) (Chutung, Hsinchu, Taiwan). All chemicals in this work were obtained as analytical grade and directly used without further purification. All aqueous solutions were prepared using a Milli-Q water purification system (Millipore, Milford, MA, USA).

2.2. Preparation of *gra@SiC/Ni-Co-O*

First, 10 mg of SiC and graphite conductive additive are uniformly dispersed via ultra-sonication for 1 h to make well-dispersed and homogenous suspensions. A graphite electrode with a 3 mm diameter was used for surface modification. Then, 10 μL of SiC homogeneous suspension with a concentration of 3 mg mL^{-1} was modified on the graphite electrode surface by a drop coating method and dried the SiC modified electrode under 60 °C for 30 min. Graphite electrodes without and with SiC modification were designated as *gra* and *gra@SiC*, respectively. Subsequently, the *gra/Ni-Co-O* and *gra@SiC/Ni-Co-O* were fabricated through the electrodeposition method by applying a constant potential at room temperature. The electrodeposition method was performed potentiostatically with an electrochemical analyzer using a three-electrode system. The three-electrode system was used consisting of *gra* and *gra@SiC* as working electrode, a platinum wire as counter electrode, and an Ag/AgCl (3 M KCl) as reference electrode (the volume of precursor electrolyte for electrodeposition was 20 mL). The electrodeposition precursor electrolyte of 20 mL was a mixture of $\text{Ni}(\text{NO}_3)_2 \cdot 6\text{H}_2\text{O}$ (6 mM) and $\text{Co}(\text{NO}_3)_2 \cdot 6\text{H}_2\text{O}$ (12 mM) and the mixture solution was continuously stirred at room temperature for 10 min to form a homogeneous solution. And, the precursor electrolyte was kept at room temperature for the subsequent Ni-Co hydroxide precursor electrodeposition. Then, *gra* and *gra@SiC* working electrodes were immersed in the precursor electrolyte. The electrodeposition of Ni-Co hydroxide precursor at a constant potential of -0.6 V for 240 s, and washed with DI water trice for 15 min each, and then dried in an oven to remove the remaining reagents and collected for subsequent characterization. The resulting modified electrode was designated as *gra/Ni-Co-O* and *gra@SiC/Ni-Co-O*, respectively.

2.3. Characterization

The morphology was characterized using a Field emission scanning electron microscopic (FESEM, JSM-7800F, JEOL, Akishima, Japan) and high-resolution transmission electron microscopy (HRTEM, JEM-2010, JEOL, Japan) with selected area electron diffraction (SAED) and energy dispersive X-ray spectroscopy (EDS). Raman spectra were characterized using an automated Raman spectrometer equipped with an argon laser excitation wavelength of 532 nm (Unidron, CL Technology Co., Ltd., New Taipei city, Taiwan). The chemical structure and composition were determined by X-ray photoelectron spectroscopy (XPS, PHI-5000 Versaprobe, ULVAC-PHI, Chigasaki, Kanagawa, Japan). Electrochemical measurements were performed using a three-electrode system by an electrochemical analyzer (Autolab, model PGSTAT30, Eco Chemie, Utrecht, The Netherlands). The supercapacitor with a conventional three-electrode system comprised *gra/Ni-Co-O* and *gra@SiC/Ni-Co-O* working electrode, a platinum wire counter electrode, and an Ag/AgCl (3 M KCl) reference electrode in 1 M KOH electrolyte (pH 13.8) (the volume of KOH electrolyte for electrochemical measurements was 20 mL). The electrochemical measurements of *gra/Ni-Co-O* and *gra@SiC/Ni-Co-O* were examined by cyclic voltammetry (CV) and galvanostatic charge-discharge (GCD).

3. Results

The surface morphologies of gra, gra@SiC, gra/Ni-Co-O, and gra@SiC/Ni-Co-O were characterized using field emission scanning electron microscopy (FESEM). Compared to that of gra (Figure 1a), a notable apophysis was observed on the surface of the coating material after the addition of SiC (Figure 1b); marked in the region of the orange dashed circle), and SiC was observed to exhibit a spherical structure with a size of few tens of micrometers. Next, gra and gra@SiC were used as growth templates for the electrodeposition growth of ternary Ni-Co-O nanosheets. The SEM image confirmed the dense and even coverage of the entire surface of gra and gra@SiC by the ternary Ni-Co-O nanosheets (Figure 1c,d). Further, high-magnification FESEM images (Figure 1e,f) revealed that the ternary Ni-Co-O nanosheets formed a uniformly interconnected network with gra and gra@SiC (enlarged view of the yellow framed region in Figure 1c,d). This well-defined interconnected network structure formed a conductive network for the transport of electrons, indicating its significant potential in supercapacitors. Additionally, the SEM images revealed the aggregation tendency of the ternary Ni-Co-O nanosheets on the surface of gra in gra/Ni-Co-O, and the average diameter of the Ni-Co-O nanosheet aggregates was approximately 1 μm . In contrast, the ternary Ni-Co-O nanosheets in gra@SiC/Ni-Co-O were well-dispersed on the surface of the SiC without notable aggregation, resulting in increased surface area. Consequently, this is expected to further accelerate the electron/ion transport, thus enhancing their electrochemical performances. Further, gra/Ni-Co-O and gra@SiC/Ni-Co-O were further characterized using Raman, high-resolution transmission electron microscopy (HRTEM), and X-ray photoelectron spectroscopy (XPS).

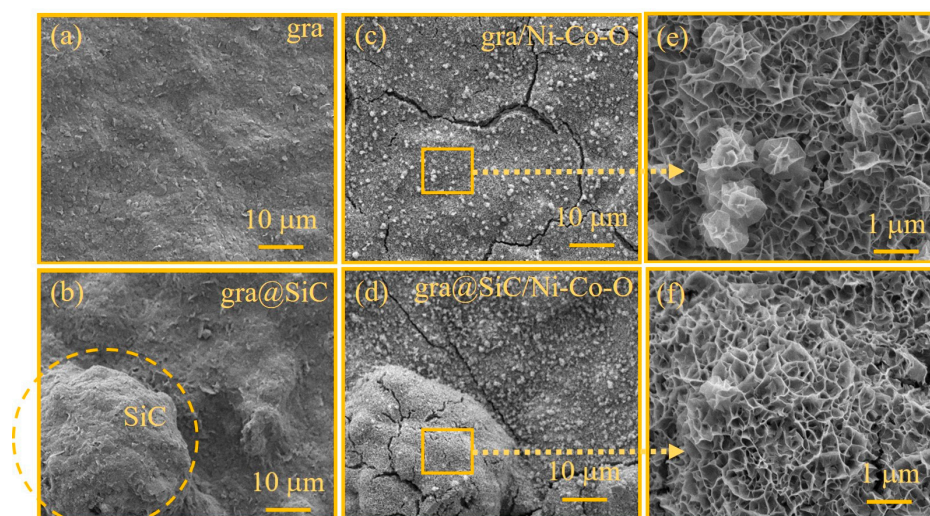


Figure 1. FESEM images of (a) gra, (b) gra@SiC, (c) gra/Ni-Co-O, and (d) gra@SiC/Ni-Co-O; (e,f) the enlarged area of the marked place in (c,d).

The phase composition and structural features of gra, gra@SiC, gra/Ni-Co-O, and gra@SiC/Ni-Co-O were characterized using Raman spectroscopy in the Raman shift range of 100–2000 cm^{-1} . Two characteristic peaks were observed at approximately 1567 (G band) and 1347 cm^{-1} (D band) in the Raman spectra of all samples and can be attributed to the presence of graphite conductive additive (gra) during the electrode slurry preparation (Figure 2). The D and G bands correspond to disordered carbon and graphitic sp^2 carbon, respectively. Additionally, a notable characteristic peak was observed in the Raman spectrum of gra@SiC at approximately 785 cm^{-1} , indicating the presence of hexagonal (mainly, 2H-SiC) polytype form phase within the gra@SiC [13], implying the successful coordination of SiC with graphite conductive additive to form gra@SiC. During the electrodeposition process, Ni-Co-O nanosheets uniformly covered the surface of gra and gra@SiC to form an interconnected structure. It is well known that the characteristic peaks observed in the

low Raman shift region of the Raman spectrum are associated with Ni–Co compounds. The characteristic peak of 2H-SiC was observed to disappear in the Raman spectra of gra/Ni–Co–O and gra@SiC/Ni–Co–O (Figure 2), and four newly formed characteristic peaks were observed at approximately 196, 468, 522, and 666 cm^{-1} , corresponding to the E_g mode, O–M–O bending, M–O A_g vibrations, and A_g modes of Ni–Co binary hydroxides, respectively. Additionally, a weak and broad band observed at approximately 1070 cm^{-1} was linked with the presence of residual nitrate ions from the nitrate precursor [14,15]. These results confirmed the successful synthesis of Ni–Co compounds with Ni–Co binary hydroxides structure by the electrodeposition process and the complete coverage of gra and gra@SiC by Ni–Co binary hydroxides.

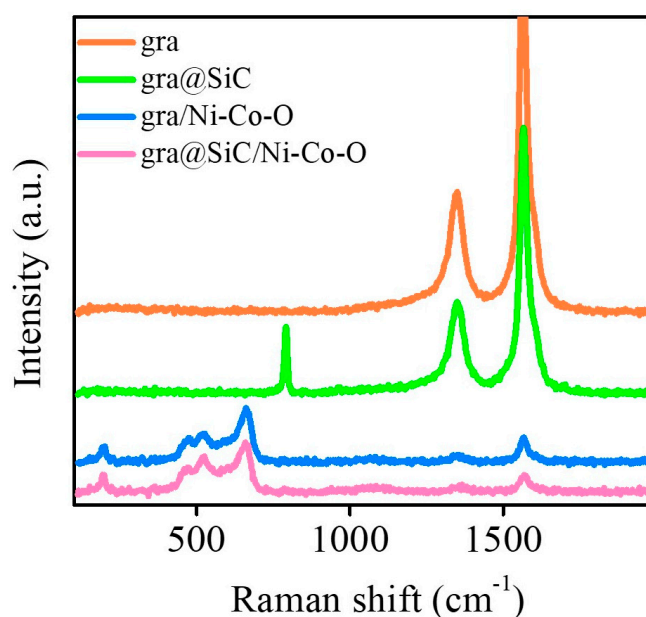


Figure 2. Raman spectra of gra, gra@SiC, gra/Ni–Co–O, and gra@SiC/Ni–Co–O.

To evaluate the Ni–Co–O nanosheet that grew along the outer wall of gra@SiC, the morphologies and relevant element compositions of gra@SiC/Ni–Co–O (the interior and exterior surfaces of the Ni–Co–O nanosheet shell, designated Pt1 and Pt2, respectively) were characterized using HRTEM, and corresponding selected area electron diffraction (SAED) pattern and energy dispersive X-ray spectroscopy (EDS), (Figure 3). A thin layer of Ni–Co–O nanosheet was conformally grown along the outer wall of gra@SiC (Figure 3a,b). SAED (Figure 3c) showed well-defined polymorphic rings confirming the polycrystalline nature of Ni–Co–O nanosheet shell. The broadening of the diffraction SAED rings suggested that the Ni–Co–O nanosheet shell was comprised of nanocrystalline or had a relatively high degree of crystallinity. The lattice planes of (100), (101), and (110) were indexed from SAED rings, which confirmed that the Ni–Co–O nanosheet shell was in the phases of Ni–Co binary hydroxides, in agreement with Raman results (Figure 2) [16,17]. In the EDS results (Figure 3d), the two selected regions of the interior and exterior surfaces within the Ni–Co–O nanosheet shell enclosed by the HRTEM image indicated that the interior surfaces of the Ni–Co–O nanosheet (Pt2) exhibited significantly higher amount of Si element than the exterior surfaces (Pt1). Additionally, it revealed the presence of Ni, Co, and O elements in the two selected regions where the formation of a uniform interconnected network structure was confirmed, indicating the strong coupling between Ni–Co–O nanosheet and the SiC. The EDS results were consistent the aforementioned results. Indeed, the inset in Figure 3d showed the atomic ratio of Ni and Co elements in the two selected regions (Pt1 and Pt2). The Ni:Co atomic ratio at Pt1 is 1.0:2.0 higher than that of the atomic ratio at Pt2 (1.0:3.5). The result further revealed that the dissimilar growth rates of the Ni–Co binary hydroxides observed in the interior and exterior surfaces of the Ni–Co–O nanosheet shell.

It can be concluded that the contact interface between the SiC core/Ni–Co–O nanosheet shell, and the surface characteristics of SiC were decisive factors influencing the growth rates of the Ni–Co binary hydroxides.

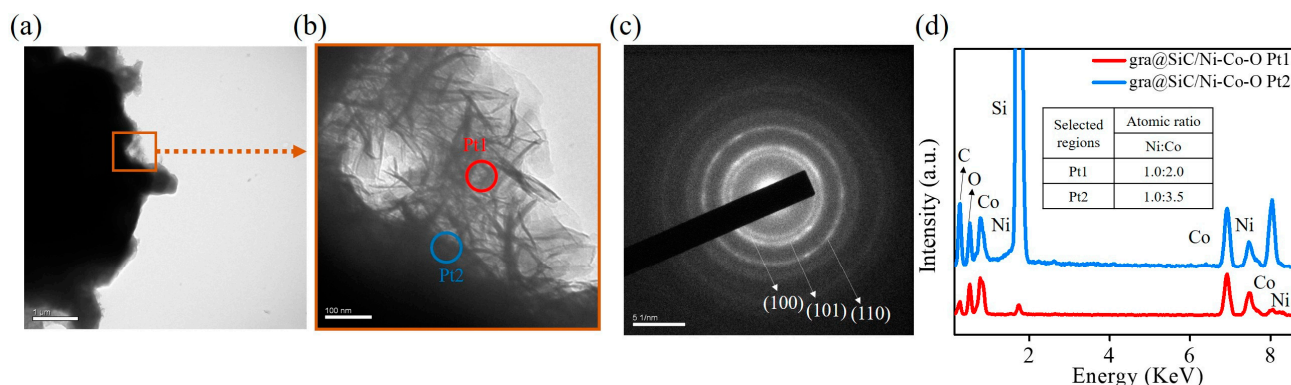


Figure 3. HRTEM images of (a) gra@SiC/Ni–Co–O, (b) the enlarged area of the marked place in (a). (c) SAED pattern. (d) EDS of the two selected regions (Pt1 and Pt2) enclosed in (b) and the inset in (d) represents the atomic ratio of Ni and Co elements.

The surface elemental composition and valance states of gra/Ni–Co–O and gra@SiC/Ni–Co–O were characterized using XPS, and the XPS results are shown in Figure 4. Figure 4a,b shows the high-resolution Ni 2p XPS profiles of gra/Ni–Co–O and gra@SiC/Ni–Co–O. Two spin–orbit-split doublets (Ni 2p_{1/2} and Ni 2p_{3/2}) were observed in the Ni 2p XPS profiles. To identify the specific Ni species, Ni 2p_{1/2} (Ni 2p_{3/2}) doublets were assigned to two fitted peaks located at approximately 872.7 (854.7 eV) and 873.8 eV (856.1 eV), which correspond to Ni²⁺ and Ni³⁺, respectively, and their shake-up satellite (Sat.) was located at approximately 880.0 eV (862.2 eV). The Ni 2p XPS quantitative analysis results are summarized in Table 1. The intensity ratio of Ni²⁺/Ni³⁺ for gra/Ni–Co–O and gra@SiC/Ni–Co–O was 0.46 and 0.33 (mainly in the oxidation state of Ni³⁺), respectively, indicating that the oxidation state of Ni in gra@SiC/Ni–Co–O is higher than that in gra/Ni–Co–O [18,19]. Figure 4c,d shows the high-resolution Co 2p XPS profiles of gra/Ni–Co–O and gra@SiC/Ni–Co–O. Two spin–orbit-split doublets were observed in the Co 2p XPS profiles at binding energies of 780.8 (Co 2p_{1/2}) and 796.7 eV (Co 2p_{3/2}). The spin-doublet Co 2p_{1/2} (Co 2p_{3/2}) region was further fitted into Co²⁺ (located at about 796.7 (781.0) eV) and Co³⁺ (located at about 794.9 (779.8) eV). The results revealed that Co²⁺ was the main oxidation state of Co on both gra/Ni–Co–O and gra@SiC/Ni–Co–O. The Co 2p XPS quantitative analysis results (Table 2) indicate the presence of more Co³⁺ species on the gra@SiC/Ni–Co–O sample [20,21]. The XPS results confirmed the formation of more Ni³⁺ and Co³⁺ active species on the surface gra@SiC/Ni–Co–O compared to gra/Ni–Co–O. Figure 4e,f shows the high-resolution O 1s XPS profiles of gra/Ni–Co–O and gra@SiC/Ni–Co–O. The O 1s XPS profile was deconvoluted into four peaks located at binding energies of peaks at 532.5, 531.3, 530.5, and 529.1 eV, respectively, which are assigned to physical/chemical adsorbed water (H–O–H), oxygen defective site (O-defect site), hydroxyl groups (M–O–H) and metal–oxygen bonds (M–O–M) on the surface of Ni–Co–O nanosheet. The O 1s XPS quantitative analysis results (Table 3) revealed reveal that both gra/Ni–Co–O and gra@SiC/Ni–Co–O possessed abundant and accessible oxygen vacancies, indicating the existence of low coordinated metal oxygen structures, which are very helpful for enhanced supercapacitive performance [22,23].

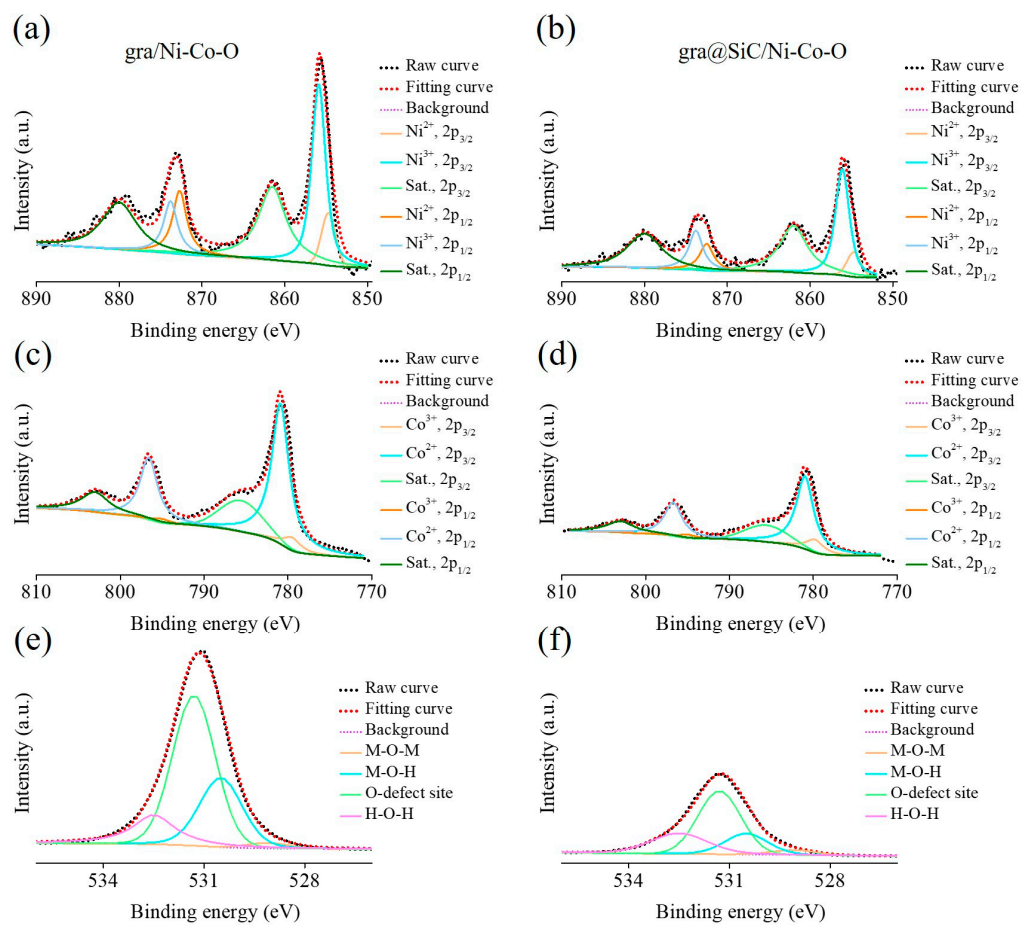


Figure 4. (a) Ni 2p, (c) Co 2p, and (e) O 1s XPS spectra of gra/Ni–Co–O. (b) Ni 2p, (d) Co 2p, and (f) O 1s XPS spectra of gra@SiC/Ni–Co–O.

Table 1. Fitted Ni 2p XPS spectra results of gra/Ni–Co–O and gra@SiC/Ni–Co–O.

Sample	Fitted Results of Ni (2p) XPS Spectra						Ni ²⁺ /Ni ³⁺
	Ni ²⁺	Ni ³⁺	Sat.	Ni ²⁺	Ni ³⁺	Sat.	
	2p _{3/2} (%)	2p _{3/2} (%)	2p _{3/2} (%)	2p _{3/2} (%)	2p _{3/2} (%)	2p _{3/2} (%)	
gra/Ni–Co–O	5.9	27.9	25.3	11.2	9.4	20.3	0.46
gra@SiC/Ni–Co–O	4.8	26.9	26.5	7.7	11.3	22.8	0.33

Table 2. Fitted Co 2p XPS spectra results of gra/Ni–Co–O and gra@SiC/Ni–Co–O.

Sample	Fitted Results of Co (2p) XPS Spectra						Co ²⁺ /Co ³⁺
	Co ³⁺	Co ²⁺	Sat.	Co ³⁺	Co ²⁺	Sat.	
	2p _{3/2} (%)	2p _{3/2} (%)	2p _{3/2} (%)	2p _{3/2} (%)	2p _{3/2} (%)	2p _{3/2} (%)	
gra/Ni–Co–O	4.2	46.6	16.8	1.3	20.6	10.5	12.27
gra@SiC/Ni–Co–O	7.4	43.4	16.3	2.1	20.1	10.7	6.74

Table 3. Fitted O 1s XPS spectra results of gra/Ni–Co–O and gra@SiC/Ni–Co–O.

Sample	Fitted Results of O (1s) XPS Spectra			
	M-O-M (%)	M-O-H (%)	O-Defect Site (%)	H-O-H (%)
gra/Ni–Co–O	2.0	27.0	55.4	15.6
gra@SiC/Ni–Co–O	4.0	18.7	52.2	25.1

To evaluate the capacitive performance of gra/Ni–Co–O and gra@SiC/Ni–Co–O, cyclic voltammetry (CV) and galvanostatic charges/discharge (GCD) measurements were performed from 0.0 to 0.6 V versus Ag/AgCl in 1 M KOH solution. The CV curves of all Ni–Co–O@3D Ni-x samples at a scan rate of 50 mV s⁻¹ exhibited a distorted semi-rectangular shape, indicating pseudocapacitance characteristics, which could be attributed to the reversible redox couple of Ni–Co–O nanosheet (Figure 5a). Moreover, the CV curve area of gra@SiC/Ni–Co–O (Figure 5a) was larger than that of gra/Ni–Co–O, indicating the excellent electrochemical capacitance performance of gra@SiC/Ni–Co–O, which can be attributed to the synergistic effects between the Ni–Co–O nanosheets and silicon carbide microspheres. The exposed Ni–Co–O nanosheet interfaces offer a large specific surface area, which could enhance the electrocatalytic active sites to accelerate electron/ion transfer characteristics. Figure 5b shows the CV curve of gra@SiC/Ni–Co–O at different scan rates. At a higher scan rate of 100 mV s⁻¹, the CV curve exhibited a slightly distorted shape, but still maintained its semi-rectangular CV shape, demonstrating its good capacitance behavior. Figure 5c,d displays the GCD curve of gra/Ni–Co–O and gra@SiC/Ni–Co–O at different current densities. The areal capacitance can be calculated from the above GCD results by the equation $C = (I \Delta t) / \Delta V$, where C is the areal capacitance (mF cm⁻²); I is the current density (mA cm⁻²); Δt is the discharge time (s); and ΔV is the voltage change during discharge (V). Rather than a triangular distribution, the GCD curves of both samples exhibited a quasi-triangular symmetrical distribution with plateaus, indicating the synergistic effect between the pseudocapacitance (Ni–Co–O nanosheets) and EDLC (SiC microspheres) behaviors. Additionally, the maximum areal capacitance of gra@SiC/Ni–Co–O (521 mF cm⁻²) was higher than that of gra/Ni–Co–O (322 mF cm⁻²) at a low current density of 1.4 mA cm⁻². In particular, the capacitive performance of gra@SiC/Ni–Co–O was higher or comparable to those of other previously reported results on combining semiconductor materials to obtain composite electrode materials (Table 4) [24–27]. This excellent performance of gra@SiC/Ni–Co–O may be attributed to the following reasons: (1) gra@SiC functioned as a conductive template for the subsequent growth of Ni–Co–O nanosheets to form a binder-free 3D well-designed hierarchical interconnected network between the Ni–Co–O nanosheets and SiC microspheres, leading to improved electrochemical performance [28]. (2) The contact interface between the SiC core/Ni–Co–O nanosheet shell, and the surface characteristics of SiC were decisive factors influencing the growth rates of the Ni–Co binary hydroxides. The Ni:Co atomic ratio at the interior surface of the Ni–Co–O nanosheet shell was higher than that at the exterior surface of the Ni–Co–O nanosheet shell, indicating that a relatively large amount of Ni hydroxide was present within gra@SiC/Ni–Co–O compared with gra/Ni–Co–O. This difference may affect supercapacitor performance [29]. (3) gra@SiC/Ni–Co–O possessed abundant oxygen vacancies and further exposed rich electroactive sites, providing dense diffusion channels for energy storage [30]. (4) The synergistic effects of EDLC (SiC microspheres) and pseudo-capacitance (Ni–Co–O nanosheets) effectively enhanced the supercapacitive performance. This study revealed that the use of SiC as the growth template prevented the aggregation of Ni–Co–O nanosheets, which can largely improve the specific surface area. Ni–Co–O nanosheets simultaneously possess pseudo-capacitive energy storage efficiency through the multiple oxidation states/structures of Ni and Co atoms, resulting in improved supercapacitive performance [31].

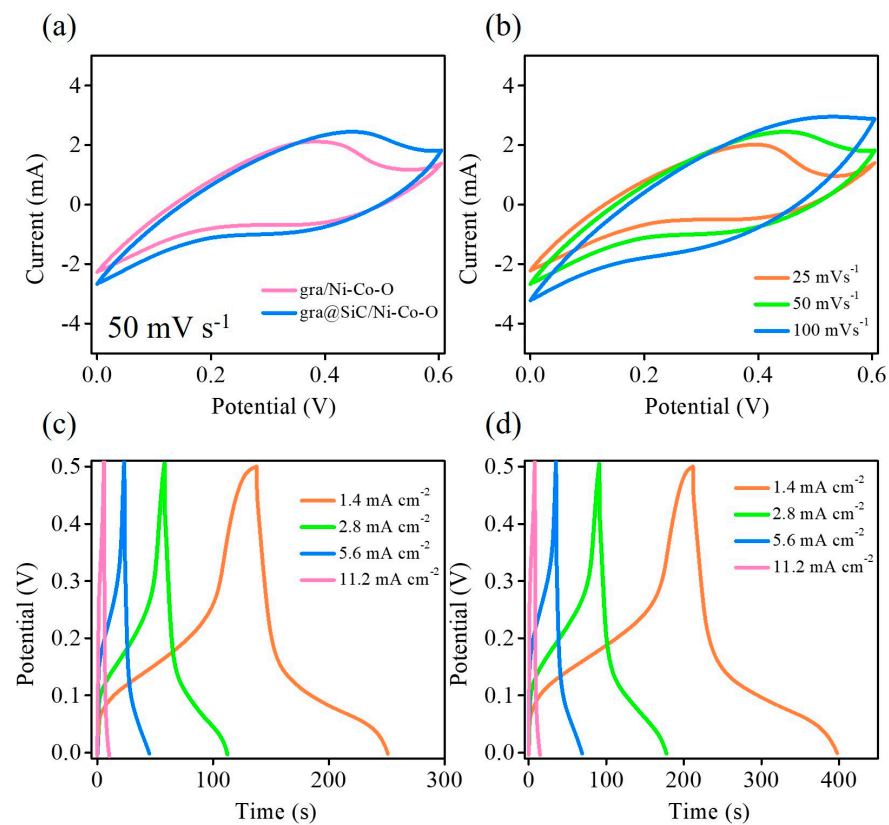


Figure 5. (a) Cyclic voltammetry of gra/Ni-Co-O, and gra@SiC/Ni-Co-O. (b) Cyclic voltammetry of gra@SiC/Ni-Co-O at different scan rates. Galvanostatic charge/discharge of (c) gra/Ni-Co-O and (d) gra@SiC/Ni-Co-O at different current densities.

Table 4. Comparing the performance of semiconductor materials-based supercapacitors.

Samples	Electrolyte	Current Density (mA cm ⁻²)	Areal Capacitance (mF cm ⁻²)	Reference
gra@SiC/Ni-Co-O	KOH (1 M)	1.4	521	This work
SiC@PANI	H ₂ SO ₄ (1 M)	1	352	[24]
SiC@SiO ₂ /MnO ₂	Na ₂ SO ₄ (1 M)	0.2	271	[25]
SiC/HG/MnO ₂	LiCl (3 M)	7.2	1000	[26]
SiNWs/NC@NiO	KOH (6 M)	1	110	[27]

To further understand the stability and the charge storage mechanisms of gra@SiC/Ni-Co-O after electrochemical testing, the electrochemical behavior of gra@SiC/Ni-Co-O before and after electrochemical testing was evaluated using FESEM and XPS (Figure 6). Figure 6a shows the FESEM images of gra@SiC/Ni-Co-O after electrochemical testing. The morphology of gra@SiC/Ni-Co-O after electrochemical testing indicated its structural stability, as the electrochemical testing had no effect on its morphology. The gra@SiC/Ni-Co-O possessed a 3D interconnected network with high mechanical strength, which makes the electrode more stable with electrochemical cycling. Figure 6b,c further revealed that gra@SiC/Ni-Co-O promotes the formation of a larger amount of Ni²⁺ and Co³⁺ after electrochemical testing. Interestingly, it was apparent that the opposite tendency was observed in both Ni and Co oxidation states near the surface. The Ni oxidation states were partially reduced to Ni²⁺, and the Co oxidation states were partially oxidized to Co³⁺ (see XPS results in Figures 4 and 6). This phenomenon provided strong evidence that gra@SiC/Ni-Co-O underwent an electrochemically driven phase transition, and, simultaneously, reversible redox couples of Ni²⁺/Ni³⁺ and Co²⁺/Co³⁺ occurred on or

near the surface of gra@SiC/Ni-Co-O to contribute remarkable pseudocapacitance [32,33]. The tests mentioned above can aid the understanding of charge-storage mechanisms in gra@SiC/Ni-Co-O. Gra@SiC/Ni-Co-O exhibited excellent synergistic effects of EDLC (SiC microspheres) and pseudo-capacitance (Ni-Co-O nanosheets) to synergistically enhance the capacitive performance. SiC microspheres contributed to the formation of the 3D interconnected network between Ni-Co-O nanosheets and SiC microspheres, which enlarged the large accessible surface area for charge absorption and accumulation to exhibit excellent EDLC performance. Faraday redox reaction contributed by Ni-Co-O nanosheets. The coexistence of $\text{Ni}^{2+}/\text{Ni}^{3+}$ and $\text{Co}^{2+}/\text{Co}^{3+}$ redox couples in interconnected 3D Ni-Co-O nanosheets network on SiC microspheres enabled excellent multiple redox reactions. Due to the unique synergistic effect of SiC microspheres and Ni-Co-O nanosheets, gra@SiC/Ni-Co-O significantly improved its capacitive performance and cycling stability during the charging/discharging processes.

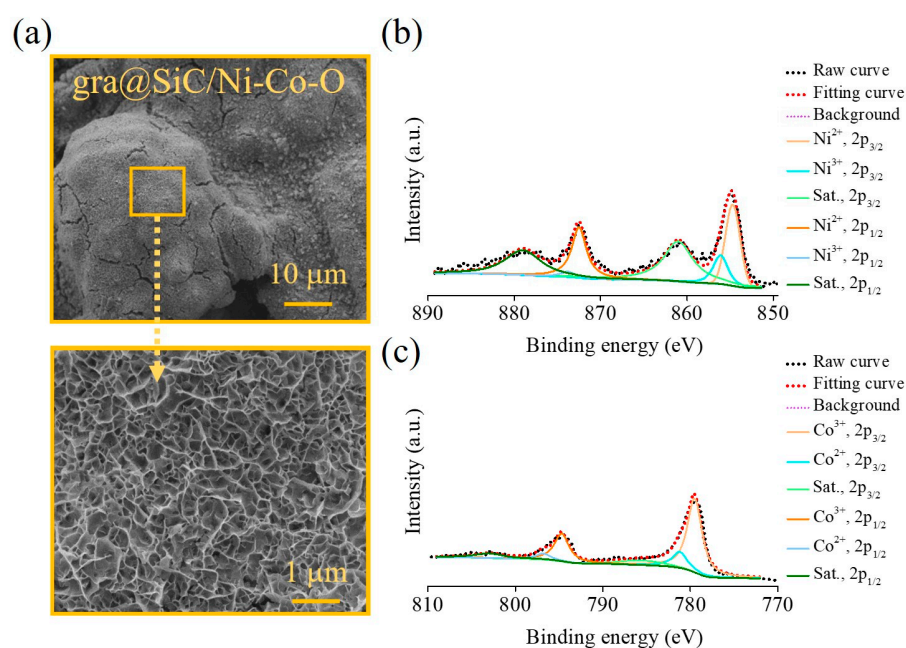


Figure 6. (a) FESEM images, (b) Ni 2p XPS spectra, and (c) Co 2p XPS spectra of gra@SiC/Ni-Co-O after electrochemical testing.

4. Conclusions

In this study, ternary Ni-Co-O nanosheets are directly grown on silicon carbide microspheres/graphite composite (gra@SiC/Ni-Co-O) by optimizing the electrodeposition method. The surface characteristics endowed SiC with the capability as growth templates for the electrodeposition growth of ternary Ni-Co-O nanosheets to construct a binder-free 3D well-designed hierarchical interconnected network structure of gra@SiC/Ni-Co-O. The gra@SiC/Ni-Co-O electrode materials own several advantages including: (1) 3D interconnected network enables enhanced mechanical properties. (2) The surface characteristics of SiC possess the difference in the growth rate of the Ni-Co binary hydroxides. A relatively large amount of Ni hydroxide was present within gra@SiC/Ni-Co-O compared with gra/Ni-Co-O. (3) The abundant and accessible oxygen vacancies lead to low coordinated metal oxygen structures. (4) The synergistic effects between two components (Ni-Co-O nanosheets and silicon carbide microspheres) contribute to faradaic redox reactions and EDLC properties. Based on the above advantages, the gra@SiC/Ni-Co-O could exhibit excellent supercapacitive performance. Further, FESEM and XPS results were used to evaluate the electrochemical behavior of gra@SiC/Ni-Co-O before and after electrochemical testing. It demonstrated that SiC microspheres contribute to the formation of the 3D interconnected network between Ni-Co-O nanosheets and SiC microspheres, improving the

cycling stability during the charging/discharging processes. And, the pseudo-capacitive charge storage mechanism in gra@SiC/Ni–Co–O involves electrochemically driven phase transition and reversible redox couples of $\text{Ni}^{2+}/\text{Ni}^{3+}$ and $\text{Co}^{2+}/\text{Co}^{3+}$ occurred on or near the surface of gra@SiC/Ni–Co–O. The as-fabricated gra@SiC/Ni–Co–O exhibited excellent capacitive performance and is a potential candidate for future electrochemical energy storage applications (lithium batteries, metal-air batteries, fuel cells, and supercapacitors), which can meet key expectations to integrate renewable energy into electrical grid systems.

Author Contributions: Conceptualization, H.-W.C., K.-C.C., T.-Y.L. and Y.-C.T.; methodology, H.-W.C., K.-C.C. and T.-Y.L.; software, Z.-Y.T. and J.-J.Y.; formal analysis, H.-W.C., Z.-Y.T. and J.-J.Y.; investigation, H.-W.C., Z.-Y.T., J.-J.Y., K.-C.C., T.-Y.L. and Y.-C.T.; data curation, H.-W.C., Z.-Y.T. and J.-J.Y.; writing—original draft preparation, H.-W.C. and Y.-C.T.; writing—review and editing, H.-W.C. and Y.-C.T.; visualization, H.-W.C.; supervision, H.-W.C.; project administration, H.-W.C. and Y.-C.T. All authors have read and agreed to the published version of the manuscript.

Funding: This research was funded by the National Science and Technology Council (NSTC), the National United University (NUU), the Ministry of Economic Affairs (MEA), and the Industrial Technology Research Institute/Material and Chemical Laboratories (ITRI/MCL), Taiwan (NSTC 112-2221-E-239-001-MY3, NSTC 112-2221-E-005-007-MY3, SE112002, and 112-EC-17-A-24-1771).

Data Availability Statement: Not applicable.

Acknowledgments: The authors are grateful to the NSTC, NUU, MEA, and ITRI/MCL for the financial assistance granted in support of this work. For instrumentation support, we thank the NSTC and the Instrument Center of National Chung Hsing University, Taiwan, for help with FESEM, HRTEM, and XPS measurements (NSTC 112-2740-M-005-001).

Conflicts of Interest: The authors declare no conflict of interest.

References

1. Minakshi, M.; Wickramaarachchi, K. Electrochemical aspects of supercapacitors in perspective: From electrochemical configurations to electrode materials processing. *Prog. Solid State Chem.* **2023**, *69*, 100390. [[CrossRef](#)]
2. Cai, D.; Xiao, S.; Wang, D.; Liu, B.; Wang, L.; Liu, Y.; Li, H.; Wang, Y.; Li, Q.; Wang, T. Morphology controlled synthesis of NiCo_2O_4 nanosheet array nanostructures on nickel foam and their application for pseudocapacitors. *Electrochim. Acta* **2014**, *142*, 118–124. [[CrossRef](#)]
3. Chen, J.; Zhang, Y.; Hou, X.; Su, L.; Fan, H.; Chou, K.-C. Fabrication and characterization of ultra light SiC whiskers decorated by RuO_2 nanoparticles as hybrid supercapacitors. *RSC Adv.* **2016**, *6*, 19626–19631. [[CrossRef](#)]
4. Gu, L.; Wang, Y.; Fang, Y.; Lu, R.; Sha, J. Performance characteristics of supercapacitor electrodes made of silicon carbide nanowires grown on carbon fabric. *J. Power Sources* **2013**, *243*, 648–653. [[CrossRef](#)]
5. Kim, M.; Kim, J. Development of high power and energy density microsphere silicon carbide– MnO_2 nanoneedles and thermally oxidized activated carbon asymmetric electrochemical supercapacitors. *Phys. Chem. Chem. Phys.* **2014**, *16*, 11323–11336. [[CrossRef](#)]
6. Oh, I.; Kim, M.; Kim, J. Fe_3O_4 /carbon coated silicon ternary hybrid composite as supercapacitor electrodes. *Appl. Surf. Sci.* **2015**, *328*, 222–228. [[CrossRef](#)]
7. Pramitha, A.; Raviprakash, Y. Recent developments and viable approaches for high-performance supercapacitors using transition metal-based electrode materials. *J. Energy Storage* **2022**, *49*, 104120. [[CrossRef](#)]
8. Dai, M.; Zhao, D.; Wu, X. Research progress on transition metal oxide based electrode materials for asymmetric hybrid capacitors. *Chin. Chem. Lett.* **2020**, *31*, 2177–2188. [[CrossRef](#)]
9. Yadav, S.; Sharma, A. Importance and challenges of hydrothermal technique for synthesis of transition metal oxides and composites as supercapacitor electrode materials. *J. Energy Storage* **2021**, *44*, 103295. [[CrossRef](#)]
10. Kim, M.; Kim, J. Redox deposition of birnessite-type manganese oxide on silicon carbide microspheres for use as supercapacitor electrodes. *ACS Appl. Mater. Interfaces* **2014**, *6*, 9036–9045. [[CrossRef](#)]
11. Kim, M.; Kim, J. Synergistic interaction between pseudocapacitive Fe_3O_4 nanoparticles and highly porous silicon carbide for high-performance electrodes as electrochemical supercapacitors. *Nanotechnology* **2017**, *28*, 195401. [[CrossRef](#)]
12. Kim, M.; Yoo, J.; Kim, J. Fast and reversible redox reaction of MgCo_2O_4 nanoneedles on porous β -polytype silicon carbide as high performance electrodes for electrochemical supercapacitors. *J. Alloys Compd.* **2017**, *710*, 528–538. [[CrossRef](#)]
13. Popov, O.; Vishnyakov, V.; Poperenko, L.; Yurglevych, I.; Avramenko, T.; Ovcharenko, A. Reactively sintered TiB_2 -based heteromodulus UHT ceramics with in-situ formed graphene for machinable concentrated solar light absorbers. *Ceram. Int.* **2022**, *48*, 17828–17836. [[CrossRef](#)]
14. Liang, J.; Xiang, C.; Zou, Y.; Hu, X.; Chu, H.; Qiu, S.; Xu, F.; Sun, L. Spacing graphene and Ni-Co layered double hydroxides with polypyrrole for high-performance supercapacitors. *J. Mater. Sci. Technol.* **2020**, *55*, 190–197. [[CrossRef](#)]

15. Adán-Más, A.; Duarte, R.G.; Silva, T.M.; Guerlou-Demourgues, L.; Montemor, M.F.G. Enhancement of the Ni-Co hydroxide response as energy storage material by electrochemically reduced graphene oxide. *Electrochim. Acta* **2017**, *240*, 323–340. [[CrossRef](#)]
16. Zhou, X.-C.; Yang, X.-Y.; Fu, Z.-B.; Yang, Q.; Yang, X.; Tang, Y.-J.; Wang, C.-Y.; Yi, Y. Single-crystalline ultrathin nanofilms of Ni aerogel with Ni(OH)₂ hybrid nanoparticles towards enhanced catalytic performance for ethanol electro-oxidation. *Appl. Surf. Sci.* **2019**, *492*, 756–764. [[CrossRef](#)]
17. Zhou, Q.; Bian, Q.; Liao, L.; Yu, F.; Li, D.; Tang, D.; Zhou, H. In situ electrochemical dehydrogenation of ultrathin Co(OH)₂ nanosheets for enhanced hydrogen evolution. *Chin. Chem. Lett.* **2023**, *34*, 107248. [[CrossRef](#)]
18. Salarizadeh, P.; Askari, M.B.; Seifi, M.; Rozati, S.M.; Eisazadeh, S.S. Pristine NiCo₂O₄ nanorods loaded rGO electrode as a remarkable electrode material for asymmetric supercapacitors. *Mater. Sci. Semicond. Process.* **2020**, *114*, 105078. [[CrossRef](#)]
19. Pore, O.; Fulari, A.; Chavare, C.; Sawant, D.; Patil, S.; Shejwal, R.; Fulari, V.; Lohar, G. Synthesis of NiCo₂O₄ microflowers by facile hydrothermal method: Effect of precursor concentration. *Chem. Phys. Lett.* **2023**, *824*, 140551. [[CrossRef](#)]
20. Xiong, D.; Du, Z.; Li, H.; Xu, J.; Li, J.; Zhao, X.; Liu, L. Polyvinylpyrrolidone-assisted hydrothermal synthesis of CuCoO₂ nanoplates with enhanced oxygen evolution reaction performance. *ACS Sustain. Chem. Eng.* **2018**, *7*, 1493–1501. [[CrossRef](#)]
21. Cai, P.; Zhao, J.; Zhang, X.; Zhang, T.; Yin, G.; Chen, S.; Dong, C.-L.; Huang, Y.-C.; Sun, Y.; Yang, D.; et al. Synergy between cobalt and nickel on NiCo₂O₄ nanosheets promotes peroxymonosulfate activation for efficient norfloxacin degradation. *Appl. Catal. B Environ.* **2022**, *306*, 121091. [[CrossRef](#)]
22. Pathak, M.; Mutadak, P.; Mane, P.; More, M.A.; Chakraborty, B.; Late, D.J.; Rout, C.S. Enrichment of the field emission properties of NiCo₂O₄ nanostructures by UV/ozone treatment. *Mater. Adv.* **2021**, *2*, 2658–2666. [[CrossRef](#)]
23. Yan, D.; Wang, W.; Luo, X.; Chen, C.; Zeng, Y.; Zhu, Z. NiCo₂O₄ with oxygen vacancies as better performance electrode material for supercapacitor. *Chem. Eng. J.* **2018**, *334*, 864–872. [[CrossRef](#)]
24. Wang, R.; Li, W.; Jiang, L.; Liu, Q.; Wang, L.; Tang, B.; Yang, W. Rationally designed hierarchical SiC@PANI core/shell nanowire arrays: Toward high-performance supercapacitors with high-rate performance and robust stability. *Electrochim. Acta* **2022**, *406*, 139867. [[CrossRef](#)]
25. Zhang, Y.; Chen, J.; Fan, H.; Chou, K.-C.; Hou, X. Characterization of modified SiC@SiO₂ nanocables/MnO₂ and their potential application as hybrid electrodes for supercapacitors. *Dalton Trans.* **2015**, *44*, 19974–19982. [[CrossRef](#)] [[PubMed](#)]
26. Chen, Y.; Zhang, X.; Xue, W.; Xie, Z. Three-dimensional SiC/holey-graphene/holey-MnO₂ architectures for flexible energy storage with superior power and energy densities. *ACS Appl. Mater. Interfaces* **2020**, *12*, 32514–32525. [[CrossRef](#)] [[PubMed](#)]
27. Zhou, Q.; Bao, M.; Ni, X. A novel surface modification of silicon nanowires by polydopamine to prepare SiNWs/NC@NiO electrode for high-performance supercapacitor. *Surf. Coat. Technol.* **2021**, *406*, 126660. [[CrossRef](#)]
28. Yu, M.; Chen, J.; Liu, J.; Li, S.; Ma, Y.; Zhang, J.; An, J. Mesoporous NiCo₂O₄ nanoneedles grown on 3D graphene-nickel foam for supercapacitor and methanol electro-oxidation. *Electrochim. Acta* **2015**, *151*, 99–108. [[CrossRef](#)]
29. Chen, J.-C.; Hsu, C.-T.; Hu, C.-C. Superior capacitive performances of binary nickel–cobalt hydroxide nanonetwork prepared by cathodic deposition. *J. Power Sources* **2014**, *253*, 205–213. [[CrossRef](#)]
30. Wei, S.; Wan, C.; Zhang, L.; Liu, X.; Tian, W.; Su, J.; Cheng, W.; Wu, Y. N-doped and oxygen vacancy-rich NiCo₂O₄ nanoglass for supercapacitor electrode. *Chem. Eng. J.* **2022**, *429*, 132242. [[CrossRef](#)]
31. Bai, Y.; Wang, R.; Lu, X.; Sun, J.; Gao, L. Template method to controllable synthesis 3D porous NiCo₂O₄ with enhanced capacitance and stability for supercapacitors. *J. Colloid Interface Sci.* **2016**, *468*, 1–9. [[CrossRef](#)]
32. Pan, C.; Liu, Z.; Li, W.; Zhuang, Y.; Wang, Q.; Chen, S. NiCo₂O₄@polyaniline nanotubes heterostructure anchored on carbon textiles with enhanced electrochemical performance for supercapacitor application. *J. Phys. Chem. C* **2019**, *123*, 25549–25558. [[CrossRef](#)]
33. Zhang, H.; Sun, C.; Xie, X. Understanding electrochemical structural degradation of NiCo₂S₄ nanoparticles in aqueous alkaline electrolyte. *Electrochim. Acta* **2023**, *466*, 143057. [[CrossRef](#)]

Disclaimer/Publisher’s Note: The statements, opinions and data contained in all publications are solely those of the individual author(s) and contributor(s) and not of MDPI and/or the editor(s). MDPI and/or the editor(s) disclaim responsibility for any injury to people or property resulting from any ideas, methods, instructions or products referred to in the content.